ChemComm

A SIFSIX-MOF constructed from a metalloligand yields enhanced stability for selective CO_2 adsorption

Journal:	*ChemComm*
Manuscript ID	CC-COM-06-2023-002683.R2
Article Type:	Communication

COMMUNICATION

A SIFSIX-MOF constructed from a metalloligand yields enhanced stability for selective CO_2 adsorption

Alberto M. Tous-Granados and Arturo J. Hernandez-Maldonado

Received 00th January 20xx,
Accepted 00th January 20xx

DOI: 10.1039/x0xx00000x

The first example of a metalloligand(*ML*)-based non-interpenetrated SIFSIX MOF $[Cu(ML)_2(SiF_6)]_n$ (*ML* = $Cu(pyac)_2$ = bis[3-(4-pyridyl)pentane-2,4-dionato]copper(II)) exhibits one-dimensional pore channels decorated with accessible Cu^{2+} sites that provide superior water vapor stability and CO_2 selectivity over CH_4 vs. similar materials constructed from non-metal containing organic ligands.

Metal-organic frameworks (MOFs) are considered potential platforms for developing adsorbents for carbon dioxide gas removal in the quest to achieve a carbon-neutral energy cycle.[1] MOFs possess molecular architectures that can be tuned to tailor adsorbate-adsorbent interactions to enhance capacity and selectivity.[2] An example is a well-known subset of hybrid pillared square MOFs initially proposed by Zaworotko and co-workers, which are assembled from square lattices (**sql**) formed by a metal node (e.g., M = Cu^{2+} or Zn^{2+}) and a bipyridyl organic linker (e.g., *L* = *dpp* = 1,4-di(4-pyridyl)phenyl) pillared by $[SiF_6]^{2-}$ (i.e., **SIFSIX**) anions to form a primitive cubic (**pcu**) framework, (i.e., $[M(L)_2(SiF_6)]_n$) (see Scheme 1A).[3, 4] An advantage of this MOF series is that the pore size/functionality can be controlled upon selecting appropriate metal centers, pillar linkers, and anion groups.[5]

Noro et al. reported a prototype SIFSIX MOF $Cu(bpy)_2(SiF_6)]_n$ variant (*bpy* = 4,4' bipyridine, see Chart S1) with pore channels of about 9.5 Å (herein and throughout this Communication, the effective pore size is reported as the diagonal distance between fluor atoms considering their van der Waals radii) with higher methane uptake compared to zeolite 13X.[6] The use of a larger organic linker (i.e., *bpe* = 1,2-Bis(4-pyridyl)ethene) (see Chart S1) afforded the $[Cu(bpe)_2(SiF_6)]_n$ variant with pores of about 12.5 Å, demonstrating that the effective pore window aperture is a crucial parameter that governs the CO_2 uptake with these materials.[7] Indeed, the use of the shortest possible bipyridyl linker *pyz* (*pyz* = pyrazine, see Chart S1) can significantly enhance CO_2 capture, even at trace concentrations, in the non-interpenetrated MOF $[Cu(pyz)_2(SiF_6)]_n$ with pores of about 3.5 Å.[8] On the other hand, the pore channel dimensions can also be tuned using longer ligand linkers (e.g., *dpa* = 4,4'-dipyridylacetylene, see Chart S1), and controlled solvent media, to yield interpenetrated frameworks, i.e. $[Cu(pyz)_2(SiF_6)]_n$-i (-i denoting interpenetration) with pores of *ca*. 5.1 Å.[9]

Nevertheless, some SIFSIX MOFs, especially the non-interpenetrated variants, lose their 3D crystallinity upon solvent guest removal, thermal heating, or exposure to water vapor.[10-12] The adsorbent stability is of utmost importance for industrial applications (e.g., a packed bed adsorber) during storage, handling, operation, and regeneration.[13] Hence, we hypothesized that a SIFSIX framework should be stabilized by reinforcing the ligand columns via the addition of a metal atom located at the middle of the dipyridyl linker, i.e., using a metalloligand (*ML* = $Cu(pyac)_2$ = bis[3-(4-pyridyl)pentane-2,4-dionato]copper(II)) instead of using an organic linker (see Scheme 1B).[14] Additionally, the resulting framework will contain

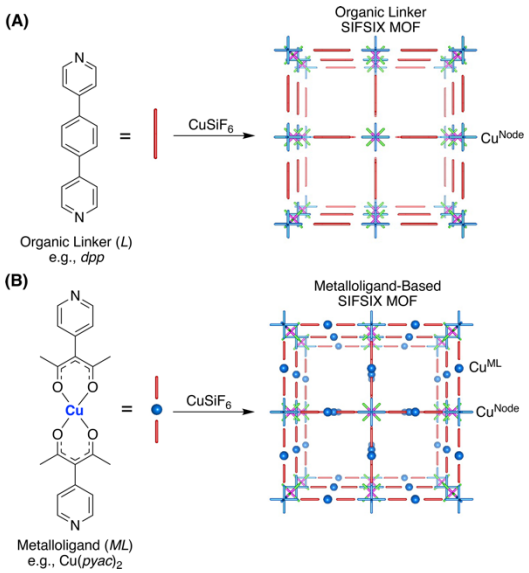

Scheme 1. Synthesis route to obtain (A) a traditional organic linker-based and (B) a metalloligand-based SIFSIX MOFs. Colour code: Cu^{Node} (blue octahedrons) Cu^{ML} (blue spheres), Si (magenta), F (green), organic linker (red).

Department of Chemical Engineering, University of Puerto Rico-Mayagüez Campus Mayagüez, PR 00681-9000; E-mail: arturoj.hernandez@upr.edu; Phone: 787-832-4040 x3748; Fax: 787-834-3655

† Electronic Supplementary Information (ESI) available: Experimental procedures, crystallographic data, TGA profiles, adsorption isotherms, isosteric heat of adsorption, and IAST calculations. CCDC 2262976. For ESI and crystallographic data in CIF or other electronic format see DOI: 10.1039/x0xx00000x

Cu^{ML} metal sites along the one-dimensional (1D) channels with more accessibility to interact with guest molecules than the Cu^{Node} sites (Scheme 1B).

Here, the $[Cu(Cu(pyac)_2)_2(SiF_6)]_n$ compound was formed by a fast reaction between a solution of $Cu(pyac)_2$ in tetrahydrofuran (*thf*) with a methanolic solution of $CuSiF_6$. Complete synthesis, characterization, and other calculation details are provided as Supplementary Information (ESI). The crystallographic structure was solved by Rietveld refinement (see Figure S1), revealing a non-interpenetrated network with distorted octahedral coordination of the Cu^{Node} by four N atoms of H*pyac* linkers to afford $[Cu(Cu(pyac)_2)_2]_n$ square lattices in the *ac* plane which are joined by $[SiF_6]^{2-}$ anions along the *b* axis (see Figure 1). As a result, one-dimensional 1D channels with accessible Cu^{ML} sites and an effective pore size of about 15.1 Å x 25.4 Å (i.e., 20.2 Å avg.) are formed along the *b* axis (see Figure 1A). There are also channels along the *c* axis with 2.1 Å x 12.8 Å dimensions considering the van der Waals radii (Figure 1B), which are perhaps not wide enough to allow easy passage of CO_2, N_2, or CH_4 molecules (i.e., kinetic diameters of 3.3 Å, 3.6 Å, and 3.8 Å, respectively). The void and pore volumes calculated from the crystallographic structure of $[Cu(Cu(pyac)_2)_2(SiF_6)]_n$ are 42% and 0.653 $cm^3\ g^{-1}$, respectively.

The thermogravimetric analysis (TGA) of $[Cu(Cu(pyac)_2)_2(SiF_6)]_n$ (Figure S2A) matches well with a material balance (in wt.%) corresponding to the initial loss of weak physisorbed water molecules from 25 to 90 °C (12.80% exp. vs. 12.20% calc.), followed by a gradual organic ligand release (67.55% exp. vs. 67.60% calc.) and a copper oxide residue (19.65% exp. vs. 20.20% calc.). It is worth noting that the TGA derivative profile (Figure S2A) does not show a double peak at the zone corresponding desorption of water, indicating that the Cu^{Node} and Cu^{ML} sites of $[Cu(Cu(pyac)_2)_2(SiF_6)]_n$ are coordinatively saturated, as opposed to a similar compound $[Cu_2(pzdc)_2(Cu(pyac)_2)]_n$ (*pzdc* = pyrazine-2,3-dicarboxylate)

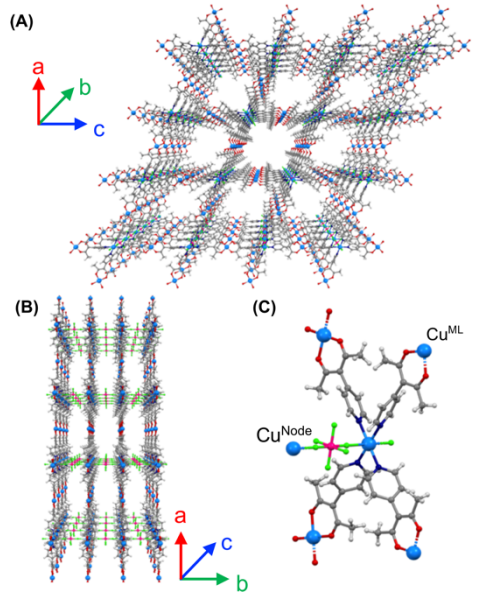

Figure 1. Perspective extended structure views of $[Cu(Cu(pyac)_2)_2(SiF_6)]_n$ (A) along the *b* axis showing the one-dimensional (1D) channels and (B) along the *c* axis. (C) Local structure around the asymmetric unit. Colour code: Cu (sky blue), Si (magenta), F (green), O (red), C (grey), H (white), N (navy blue).

reported by Sakamoto et al.[15] Also, $[Cu(Cu(pyac)_2)_2(SiF_6)]_n$ is more thermally resistant compared to the $Cu(bpy)_2(SiF_6)]_n$ variant that decomposes at *ca*. 150 °C (see Figure S2C-D).[16] The in-situ high-temperature X-ray diffraction (XRD) profiles show no peaks after 230 °C (Figure S2B), which is in good agreement with observations from the TGA profile (Figure S2A).

A closer look at the in-situ high-temperature XRD data (Figure S3) reveals an increase in the distance (*d*-spacing) between layers parallel to the *bc* planes as the temperature increases. The displacement is about 0.3 and 0.1 Å for the (100) and (200) planes, respectively. Such a flexible-like behavior could be attributed to subtle changes in the coordination environment of the copper atoms as the solid losses physisorbed guest molecules.[17] For this reason, the textural properties of $[Cu(Cu(pyac)_2)_2(SiF_6)]_n$ were assessed at different temperatures ranging from -196 to 25 °C and variable equilibration times (Figure S4 and Table S3). At cryogenic temperatures (i.e., N_2 at -196 °C and CO_2 at -78 °C (Figure S4)), the single component adsorption isotherms are of type I, typical of a microporous compound. The surface area and pore volume are calculated to be about 463 $m^2\ g^{-1}$ and 0.272 $cm^3\ g^{-1}$, respectively. A Horvath-Kawazoe (HK) pore volume plot (Figure S4A) shows a single, rather sharp peak at about 20 Å, denoting that the 1D pore channels are uniform and match well with the structural calculations. As the temperature increases to 25 °C, so does the pore volume, to about 0.527 $cm^3\ g^{-1}$ (see Table S3); this is closer to the value obtained from the crystallographic structural calculations at the same temperature. The behavior upon a change in temperature and CO_2 adsorption is possibly due to a flexibility of the pyrazine moieties in $Cu(pyac)_2$ that ultimately results in changes in the framework geometry.[18, 19] Also, the equilibration time-dependent and hysteretic CO_2 adsorption/desorption have been well-described for a copper-based $[Cu_2(pzdc)_2(bpy)]_n$ porous coordination polymer.[20]

The enhanced thermal stability and porosity of $[Cu(Cu(pyac)_2)_2(SiF_6)]_n$ prompted the preliminary evaluation of the performance of this material for adsorption separation applications. However, it should be noted that the CO_2 shape of the adsorption leg of CO_2 (see Figures S5A and S6A) suggests that the new material is perhaps not adequate for direct air or post-combustion capture (i.e., low relative working capacity), but a candidate for bulk separations. An example is the upgrade of biogas, which implies the separation of CO_2/CH_4 (50:50) gas mixtures at 25 °C and 1 atm.[1, 8, 21] As mentioned before, when the pore window size decreases in a SIFSIX platform, the CO_2 uptake sharply increases due to the overlapping of surface potentials and strong interactions between the CO_2 permanent quadrupole moment and the fluor atoms of the 1D channels.[22] Also, the CH_4 uptake decreases with a pore size reduction due to pore-blocking effects and the absence of a quadrupole in the guest molecules.[23] As a result, SIFSIX MOFs follow the general trend that selectivity decreases as the pore window size

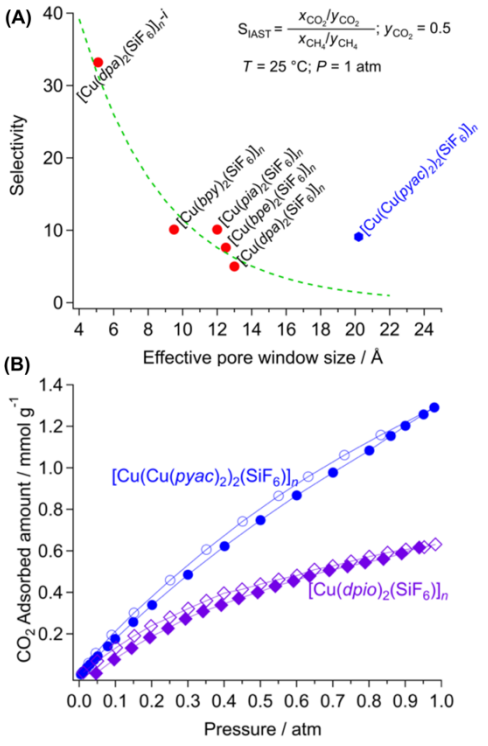

Figure 2. (A) IAST selectivity for CO_2/CH_4 (50:50) mixtures at 25 °C and 1 atm for several reported SIFSIX MOFs. (B) Single-component adsorption (filled symbols) and desorption (empty symbols) isotherms of CO_2 at 25 °C over $[Cu(Cu(pyac)_2)_2(SiF_6)]_n$ and $[Cu(dpio)_2(SiF_6)]_n$. Data for $[Cu(dpio)_2(SiF_6)]_n$ "Reprinted with permission from *J. Am. Chem. Soc.* 2014, 136, 21, 7543–7546. Copyright 2014 American Chemical Society."

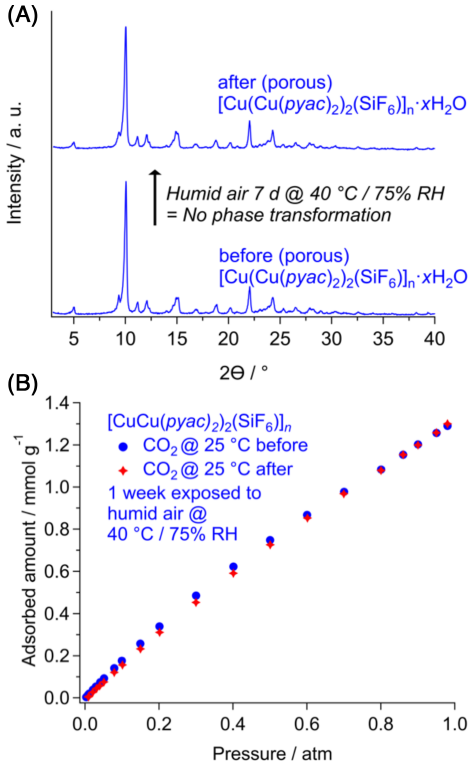

Figure 3. (A) Powder X-ray diffraction patterns before and after humidity tests, and (B) equilibrium isotherms for single component CO_2 adsorption before and after exposure to humidity for $[Cu(Cu(pyac)_2)_2(SiF_6)]_n$. XRD data were gathered at ambient temperature.

increases (Figure 2A). However, the $[Cu(Cu(pyac)_2)_2(SiF_6)]_n$ compound is an outlier considering the much larger channels compared to other variants (Figure 2A). This might be attributed to stronger interactions between the Cu^{ML} sites and the CO_2 permanent quadrupole moment, as evidenced when comparing the CO_2 uptake of $[Cu(Cu(pyac)_2)_2(SiF_6)]_n$ vs. $[Cu(dpio)_2(SiF_6)]_n$ (*dpio* = 4,7-bis(4-pyridyl)-1,1,3,3- tetramethylisoindolin-2-yloxyl) (see Figure 2B) with similar textural properties but lacking metal sites in the organic linkers.[24] Furthermore, the CO_2 isosteric heat of adsorption of $[Cu(Cu(pyac)_2)_2(SiF_6)]_n$ is 21.1 kJ/mol, significant considering the material pore size (see Table S5). The square planar coordination and accessibility of the Cu^{ML} sites (i.e., OMS) of $[Cu(Cu(pyac)_2)_2(SiF_6)]_n$ probably explains the enhanced observed guest-adsorbent interaction; a similar behavior have been documented both theoretically (i.e., density functional theory (DFT) calculations) and experimentally for an analogous MOF compound, containing Pd^{2+} square planar coordination geometry.[25] The selectivity of $[Cu(Cu(pyac)_2)_2(SiF_6)]_n$ is also higher compared to other MOF materials having 1D pore channels but lacking fluor or accessible copper atoms (see Table S5).

It has been previously reported that fluorine incorporation as functional groups can also impart enhanced water stability to metal-organic compounds.[26-29] For this reason, accelerated humid air stability tests were performed by exposing activated samples of $[Cu(Cu(pyac)_2)_2(SiF_6)]_n$ and $[Cu(bpy)_2(SiF_6)]_n$ to humid air under standard protocols conditions (i.e., 40 °C and 75% RH).[10] $[Cu(Cu(pyac)_2)_2(SiF_6)]_n$ is completely stable in humid air even after one week of exposure, as shown by XRD data and even CO_2 adsorption measurements (Figures 3A-B). In contrast, after only one day of exposure to humidity, the $[Cu(bpy)_2(SiF_6)]_n$ undergoes phase change as confirmed through XRD patterns and even a considerable decrease in CO_2 uptake (see Figure S7A-B). This irreversible phase change from porous to non-porous has been well described elsewhere and is attributed to a coordination displacement of $[SiF_6]^{2-}$ anions by water molecules (Scheme S2A).[16, 30] On the other hand, It is worth noting that a sample of $[Cu(Cu(pyac)_2)_2(SiF_6)]_n$ was also exposed for more than one month to humid air conditions (i.e., 25 °C and 65% RH) without any noticeable changes in the XRD patterns.

It is suggested that the structure of $[Cu(Cu(pyac)_2)_2(SiF_6)]_n$ preserves integrity because water molecules cannot displace the Cu^{Node}-F coordination bond (see Scheme S2B) as in the cases of $[Cu(bpy)_2(SiF_6)]_n$ or $[Cu(bpetha)_2(acetone)_2]_n{\cdot}2PF_6$ (*bpetha* = 1,2- bis(4-pyridyl)ethane).[31] It was previously reported that the water vapor stability of the interpenetrated $[Cu(dpa)_2(SiF_6)]_n$-i variant compared to $[Cu(azpy)_2(SiF_6)]_n$-i should be related to the strength of attraction forces between neighbor organic *dpa* linkers trapping the $[SiF_6]^{2-}$ anions.[10] However, this does not necessarily holds for the non-interpenetrated $[Cu(Cu(pyac)_2)_2(SiF_6)]_n$ as the distance between adjacent $Cu(pyac)_2$ pillars is not sufficient for van der Walls interactions. On the other hand, it has been reported that using organic linkers with higher basicity (i.e., pK_a) tends to yield more stable MOF frameworks.[32, 33] The pK_a of the linkers (i.e., *bpy* vs. $Cu(pyac)_2$) can be estimated from a graph-convolutional neural network model reported elsewhere.[34] In the case of $Cu(pyac)_2$, a pK_a of 5.7 denotes higher basicity compared to *bpy* (pK_a = 4.4). This should be triggered by the presence of the Cu^{ML} atoms that

act as charge stabilizers, increasing the *N*-donor capacity of the pyridyl group of Cu(*pyac*)$_2$. As a result, the Cu^{Node}-N bond strength is perhaps augmented in [Cu(Cu(*pyac*)$_2$)$_2$(SiF_6)]$_n$, which in turn stabilizes the coordination sphere of the Cu^{Node}, and preferentially coordinates to $[SiF_6]^{2-}$ anions instead of water.

In conclusion, a non-interpenetrated metalloligand-based SIFSIX MOF with large pore channels and accessible copper sites was assembled. Using a metalloligand provides insight into the development of water and thermally stable fluorinated metal-organic compounds for selective adsorption. In principle, other metals (e.g., Cu^{2+}, Zn^{2+}, Co^{2+}, Ni^{2+}), fluoride anions (TiF_6^{2-}, GeF_6^{2-}, $NbOF_5^{2-}$, etc.), and diketonate organic linkers could be used to yield mono or heterometallic fluorinated MOFs with superior water stability for industrial applications.

Author contributions

Alberto M. Tous-Granados: Conceptualization, Methodology, Investigation, Formal Analysis, Writing - original draft.

Arturo J. Hernandez-Maldonado: Conceptualization, Methodology, Investigation, Formal Analysis, Writing - review & editing, Visualization, Project administration, Funding acquisition.

Conflicts of interest

There are no conflicts to declare.

Acknowledgments

‡ The authors thankfully acknowledge the support of this research from the National Science Foundation (NSF) Partnership for Research and Education in Materials (PREM) Award DMR-1827894.

Notes and references

1. A. Schoedel, Z. Ji and O. M. Yaghi, *Nat. Energy.*, 2016, **1**, 16034.
2. N. Behera, J. Duan, W. Jin and S. Kitagawa, *EnergyChem*, 2021, **3**, 100067.
3. A. Bajpai, M. Lusi and M. J. Zaworotko, *ChemComm.*, 2017, **53**, 3978-3981.
4. S. Subramanian and M. J. Zaworotko, *Angew. Chem., Int. Ed. Engl.*, 1995, **34**, 2127-2129.
5. C. Gu, Z. Yu, J. Liu and D. S. Sholl, *ACS Appl. Mater. Interfaces.*, 2021, **13**, 11039-11049.
6. S.-i. Noro, S. Kitagawa, M. Kondo and K. Seki, *Angew. Chem., Int. Ed.*, 2000, **39**, 2081-2084.
7. S. D. Burd, S. Ma, J. A. Perman, B. J. Sikora, R. Q. Snurr, P. K. Thallapally, J. Tian, L. Wojtas and M. J. Zaworotko, *J. Am. Chem. Soc.*, 2012, **134**, 3663-3666.
8. O. Shekhah, Y. Belmabkhout, Z. Chen, V. Guillerm, A. Cairns, K. Adil and M. Eddaoudi, *Nat. Commun.*, 2014, **5**, 4228.
9. P. Nugent, Y. Belmabkhout, S. D. Burd, A. J. Cairns, R. Luebke, K. Forrest, T. Pham, S. Ma, B. Space, L. Wojtas, M. Eddaoudi and M. J. Zaworotko, *Nature*, 2013, **495**, 80-84.
10. D. O'Nolan, A. Kumar and M. J. Zaworotko, *J. Am. Chem. Soc.*, 2017, **139**, 8508-8513.
11. J.-J. Liu, Y.-J. Hong, Y.-F. Guan, M.-J. Lin, C.-C. Huang and W.-X. Dai, *Dalton Trans.*, 2015, **44**, 653-658.
12. M.-J. Lin, A. Jouaiti, N. Kyritsakas and M. W. Hosseini, *CrystEngComm*, 2009, **11**, 189-191.
13. M. Ding, X. Cai and H.-L. Jiang, *Chem. Sci.*, 2019, **10**, 10209-10230.
14. S. S. Turner, D. Collison, F. E. Mabbs and M. Halliwell, *J. Chem. Soc., Dalton Trans.*, 1997, DOI: 10.1039/A700198C, 1117-1118.
15. H. Sakamoto, R. Matsuda, S. Bureekaew, D. Tanaka and S. Kitagawa, *Chem. Eur. J*, 2009, **15**, 4985-4989.
16. S.-i. Noro, R. Kitaura, M. Kondo, S. Kitagawa, T. Ishii, H. Matsuzaka and M. Yamashita, *J. Am. Chem. Soc.*, 2002, **124**, 2568-2583.
17. R. Matsuda, R. Kitaura, S. Kitagawa, Y. Kubota, T. C. Kobayashi, S. Horike and M. Takata, *J. Am. Chem. Soc.*, 2004, **126**, 14063-14070.
18. R. Matsuda, T. Tsujino, H. Sato, Y. Kubota, K. Morishige, M. Takata and S. Kitagawa, *Chem. Sci.*, 2010, **1**, 315-321.
19. P. Kanoo, S. K. Reddy, G. Kumari, R. Haldar, C. Narayana, S. Balasubramanian and T. K. Maji, *ChemComm.*, 2012, **48**, 8487-8489.
20. K. Riascos-Rodríguez, A. J. Schroeder, M. R. Arend, P. G. Evans and A. J. Hernández-Maldonado, *Dalton Trans.*, 2014, **43**, 10877-10884.
21. S. Chaemchuen, N. A. Kabir, K. Zhou and F. Verpoort, *Chem. Soc. Rev.*, 2013, **42**, 9304-9332.
22. K. A. Forrest, T. Pham, S. K. Elsaidi, M. H. Mohamed, P. K. Thallapally, M. J. Zaworotko and B. Space, *Cryst. Growth Des.*, 2019, **19**, 3732-3743.
23. R. Kitaura, R. Matsuda, Y. Kubota, S. Kitagawa, M. Takata, T. C. Kobayashi and M. Suzuki, *J. Phys. Chem. B*, 2005, **109**, 23378-23385.
24. L. Li, R. Matsuda, I. Tanaka, H. Sato, P. Kanoo, H. J. Jeon, M. L. Foo, A. Wakamiya, Y. Murata and S. Kitagawa, *J. Am. Chem. Soc.*, 2014, **136**, 7543-7546.
25. Y. Harada, Y. Hijikata, S. Kusaka, A. Hori, Y. Ma and R. Matsuda, *Dalton Trans.*, 2019, **48**, 2545-2548.
26. S. Kumar, B. Mohan, C. Fu, V. Gupta and P. Ren, *Coord. Chem. Rev.*, 2023, **476**, 214876.
27. J. M. Park, G.-Y. Cha, D. Jo, K. H. Cho, J. W. Yoon, Y. K. Hwang, S.-K. Lee and U. H. Lee, *Chem. Eng. J.*, 2022, **444**, 136476.
28. E. Martínez-Ahumada, M. L. Díaz-Ramírez, H. A. Lara-García, D. R. Williams, V. Martis, V. Jancik, E. Lima and I. A. Ibarra, *J. Mater. Chem. A.*, 2020, **8**, 11515-11520.
29. M. L. Díaz-Ramírez, E. Sánchez-González, J. R. Álvarez, G. A. González-Martínez, S. Horike, K. Kadota, K. Sumida, E. González-Zamora, M.-A. Springuel-Huet, A. Gutiérrez-Alejandre, V. Jancik, S. Furukawa, S. Kitagawa, I. A. Ibarra and E. Lima, *J. Mater. Chem. A.*, 2019, **7**, 15101-15112.
30. S.-i. Noro, *Phys. Chem. Chem. Phys.*, 2010, **12**, 2519-2531.
31. S.-i. Noro, S. Horike, D. Tanaka, S. Kitagawa, T. Akutagawa and T. Nakamura, *Inorg. Chem.*, 2006, **45**, 9290-9300.
32. W. Xu and O. M. Yaghi, *ACS Central Science*, 2020, **6**, 1348-1354.
33. P. Lu, Y. Wu, H. Kang, H. Wei, H. Liu and M. Fang, *J. Mater. Chem. A.*, 2014, **2**, 16250-16267.
34. X. Pan, H. Wang, C. Li, J. Z. H. Zhang and C. Ji, *J. Chem. Inf. Model.*, 2021, **61**, 3159-3165.